Theoretical Analysis of Wavelength Conversion Based on Four-Wave Mixing in Light-Holding SOAs

Pei-Miin Gong, Jyh-Tsung Hsieh, San-Liang Lee, *Member, IEEE*, and Jingshown Wu, *Senior Member, IEEE*

***Abstract*—We propose to use an additional injection beam of short wavelength to enhance the wavelength conversion that utilizes the four-wave-mixing (FWM) effect in a semiconductor optical amplifier (SOA). With this scheme, the assist light can increase the saturation intensity without sacrificing the gain of an SOA, and this leads to an increase in conversion efficiency. A numerical method dealing with various FWM mechanisms, such as amplified spontaneous emission (ASE) noise, longitudinal spatial hole burning, and wavelength-dependent gain spectrum, is developed to predict the static characteristics of our scheme. The carrier densities are nonuniformly distributed along the longitudinal direction of the SOA as a result of the ASE effect, which affects the measurement of the wavelength-dependent transparent current. The effects of an assist light on saturation output power and conversion efficiency are analyzed in detail. The analysis shows that using an assist light can improve both the conversion efficiency and signal-to-background-noise ratio (SBR) for SOAs of different lengths. The degree of improvement depends on the bias condition, assist light wavelength, and the device geometry. The study for the device optimization reveals that a compromise between conversion efficiency and SBR must be made to choose the device length.**

***Index Terms*—Wavelength conversion, assist light, four-wave mixing (FWM), semiconductor optical amplifiers (SOAs).**

I. Introduction

THE use of the nonlinear mechanism of semiconductor optical amplifiers (SOAs) in advanced communication systems has been growing rapidly in recent years. One of the mechanisms to be exploited for wavelength conversion is four-wave mixing (FWM). The wavelength conversion by virtue of the FWM process in an SOA offers advantages such as multiwavelength conversion capability [1], transparency to the modulation format and data rate, and fiber dispersion compensation.. However, this technique suffers from low conversion efficiency and signal degradation caused by the amplified spontaneous emission (ASE) noise in the device.

Manuscript received May 20, 2003; revised September 19, 2003. This work was supported in part by the National Science Council and the Ministry of Education, Taiwan, under Grant NSC91-2213-E-011-074 and Grant 89E-FA06-2-4-7.

P.-M. Gong was with the Department of Electronic Engineering, National Taiwan University of Science and Technologies, Taipei, Taiwan, R.O.C. He is now with the Computer and Communications Research Laboratories, Industrial Technology Research Institute, Hsinchu,Taiwan, R.O.C.

J.-T. Hsieh and J. Wu are with the Graduate Institute of Communication Engineering and Department of Electrical Engineering, National Taiwan University, Taipei, Taiwan, R.O.C. (e-mail: jyh_tsung@pchome.com.tw).

S.-L. Lee is with the Department of Electronic Engineering, National Taiwan University of Science and Technologies, Taipei, Taiwan, R.O.C.

Digital Object Identifier 10.1109/JQE.2003.820833

To raise the FWM conversion efficiency in SOAs, an ultrafast relaxation-related gain process is dominant [2]. As a rule of thumb, $\eta_{\mathrm{CE,max}} \propto G_0 \cdot P_{\mathrm{sat}}^2$ is a good measure to obtain high FWM conversion efficiency [3]. G_0 is the unsaturated gain and P_{sat} is the saturation power of the SOA. In general, increasing the gain and/or saturation power will enhance the conversion efficiency. The fact that P_{sat} is inversely proportional to the carrier lifetime will in turn make it necessary to speed up the carrier recovery rate of the SOA.

A novel device termed a light-holding SOA (LHSOA) has been proposed to improve the carrier dynamics through the injection of an external assist light [4]. The assist-light wavelength is typically chosen to be located in the gain region [5] or toward the transparent wavelength [4], [6]. In the latter case, the saturation power will increase without sacrificing the gain. We have demonstrated experimentally [7] that the saturation intensity and FWM wavelength conversion efficiency of an SOA could be raised with an assist light. The assist light can enhance the conversion efficiency by larger than 5 dB and the signal-to-background-noise ratio (SBR) by about 3 dB when the SOA is biased at the corresponding transparency.

In this paper, our main goals are to present a detailed analysis of the novel wavelength conversion based on the FWM and LHSOA techniques. The analysis will be used for optimizing the performance of the LHSOA technique. It can also be extended for investigating the dynamic responses of the LHSOA-based wavelength converters. We present a numerical analysis using quasi-steady-state coupled equations as well as rate equations in LHSOAs. The effects of introducing an assist light are investigated by using a comprehensive model for wavelength-dependent gain, carrier-dependent loss, and noise. The particular analysis includes the effects of carrier-density modulation (CM) or pulsation, carrier heating (CH), and spectral hole burning (SHB), which dominate the FWM interactions over bandwidths into the terahertz range [8]. We calculate the output ASE spectrum and account for the spatial dependence of the population inversion and the spectral dependence of the gain. This enables us to determine the output SBR as well as the noise figure of the conversion process.

The structure of the paper is as follows. In Section II, the static model based on FWM coupled equations and rate equations are described in detail. We investigate to elucidate the effect of ASE on amplifier gain as well as the wavelength dependence of transparent current in Section III. In Section IV, we put emphasis on the performance assessment of the SOA with the injection of an assist light. Static characteristics such as conversion efficiency

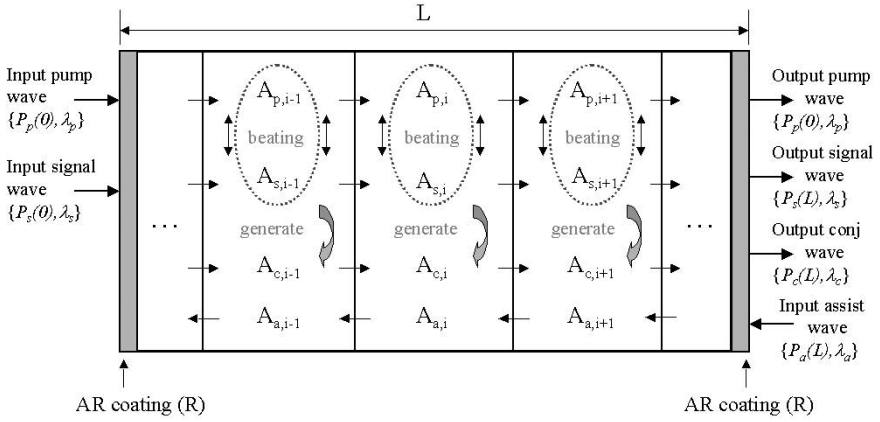

Fig. 1. Schematic diagram of the static SOA model.

and SBR are discussed here. Section V discusses the choice of the LHSOA device length with the tradeoff between the noise performance and conversion efficiency. We foresee that the assisted beam can provide larger performance enhancement for shorter devices. Finally, conclusions are given in Section VI.

II. Modeling FWM in SOAs

We have developed a numerical model to analyze the static characteristics in LHSOAs. The model is based on position-dependent rate equations for the carrier density and the optical propagation equations in both directions for the whole spectrum of ASE and injected signals. Therefore, the model accounts for a nonuniform carrier distribution and can solve both below- and above-threshold conditions. The model further includes a phenomenological expression for the total loss coefficient in the active layer, which explains the carrier-induced loss mechanisms. In addition, we also take into account both the spectral dependence and the carrier density dependence of the material gain to obtain a wavelength-dependent transparency. Fig. 1 shows a schematic of our static SOA model. The model can easily be extended to analyze large-signal dynamic responses. The SOA is assumed to have negligible reflectivity at the end facets, and therefore no reflected waves are considered.

The major role of an assist light in a LHSOA is to hold the carrier density and thus enhance the gain saturation as optical signals are injected into the device. The usual way of describing gain saturation is by relating the gain coefficient g to the optical power P by $g = g_0/(1 + P/P_{\rm sat})$, where g_0 is the unsaturated gain coefficient. Such an expression can not be applied to LHSOA since the assist light usually locates far away from the gain peak and has very different gain coefficeint from the other beams. Thus, we use the rate equation to describe the gain saturation. Besides, including the spatial distributions of the light power, carrier, and loss is critical for investigating the effects of the assist light.

A. General Formalism

To account for the interaction between carrier density N and photon density S, we divide the SOA into a number of uniform sections of length ΔL and solve the rate equation in each section. The carrier density $N_i(t)$ in section i of each SOA at time t is evaluated by the rate equation

$$\frac{dN_i}{dt} = \frac{J}{ed} - R(N_i) - \sum_{\omega} \Gamma v_g g_{m\omega,i} S_{\omega,i} - R_{\rm ASE}(N_i) \quad (1)$$

where J is the current density, e is the electron charge, d is the active region thickness, Γ is the confinement factor, v_g is the group velocity of light, g_m is the material gain, S is the average photon density, and the subscript ω stands for p, s, c, and a for the pump, signal, conjugate, and assist light, respectively. $R_{\rm ASE}$ is the ASE recombination rate. The average photon density $S_{\omega,i}$ is calculated by

$$S_{\omega,i} = \frac{|A_{\omega,i}|^2 + |A_{\omega,i+1}|^2}{2 v_g E_\omega A_{\rm cross}} \quad (2)$$

where $A_{\omega,i}$ is the traveling wave amplitudes in the unit of $(\mathrm{W})^{0.5}$ for pump, signal, conjugate, and assist light; E_ω is photon energy and $A_{\rm cross}$ is the cross-sectional area of the active layer.

The material gain is both carrier- and wavelength-dependent. In order to model the asymmetric gain profile, the gain spectrum is assumed to be cubic and the material gain is approximated by [9]

$$g_{m\omega,i} \equiv g_m(N_i, \lambda_\omega) = a_1(N_i - N_0) - a_2(\lambda_\omega - \lambda_N)^2 + a_3(\lambda_\omega - \lambda_N)^3 \quad (3)$$

where a_1, a_2, and a_3 are gain constants, N_0 is the carrier density at transparency for the peak wavelength λ_N, which is assumed to shift linearly with the carrier density, i.e., $\lambda_N = \lambda_0 - a_4 \cdot (N - N_0)$, with λ_0 being the peak wavelength at transparency. Nonlinear gain compression is included in the model through (1) where the carrier density is influenced by the total photon density of the SOA given by the stimulated emission and the ASE. Note that (3) allows us to model the wavelength-dependent transparent carrier density, for which most previous analyses fail to account.

The recombination rate depends on the carrier density and is given by

$$R(N_i) = AN_i + BN_i^2 + CN_i^3 \quad (4)$$

TABLE I
DEVICE AND MATERIAL PARAMETERS

Symbol	Description	Value	Unit
L	SOA length	1000×10^{-6}	m
w	Active layer width	1.5×10^{-6}	m
d	Active layer thickness	0.18×10^{-6}	m
A	Unimolecular recombination constant	1×10^{8}	s^{-1}
B	Bimolecular recombination constant	2.5×10^{-17}	m^3/s
C	Auger recombination constant	9.4×10^{-41}	m^6/s
a_1	Material gain constant	2.5×10^{-20}	m^2
a_2	Material gain constant	7.4×10^{18}	m^{-3}
a_3	Material gain constant	3.155×10^{25}	m^4
a_4	Material gain constant	3.0×10^{-32}	m^{-4}
N_0	Carrier density at transparency	1.5×10^{24}	m^{-3}
λ_0	Wavelength at transparency	1595×10^{-9}	m
K_0	Carrier-independent internal loss	9000	m^{-1}
K_1	Carrier-dependent internal loss	2250×10^{-24}	m^2
v_g	Group velocity	7.5×10^{7}	m/s
dn/dN	Differential refractive index	-1.2×10^{-26}	m^3
α_c	Loss in claddings	20×10^{2}	m^{-1}
α_{scat}	Scattering loss	10×10^{2}	m^{-1}
β	Spontaneous coupling factor	1×10^{-5}	--
I	Injection current	variable	A

where A is the unimolecular recombination constant caused by trapping sites, B is the bimolecular spontaneous radiative recombination coefficient, and C is the Auger recombination coefficient. The effective carrier lifetime τ_e, which includes contributions from both the spontaneous and stimulated recombination, indicates how fast the carrier density can be modulated and can be expressed by [10]

$$\frac{1}{\tau_{\rm ei}} = \frac{1}{\tau_{\rm si}} + v_g \cdot \sum_{\omega} \frac{g_{m\omega,i}\cdot\Delta L + 1}{g_{m\omega,i}\cdot\Delta L} \cdot \frac{dg_{m\omega,i}}{dN} \cdot S_{\omega,i} \quad (5)$$

where $\tau_s(=(A+2BN+3CN^2)^{-1})$ is the differential carrier lifetime equal to the inverse of the derivative of the spontaneous recombination rate to the carrier density. Obviously, the effective lifetime can be shortened by injecting an assist light.

The material loss coefficient $\alpha_a(m^{-1})$ in the active layer is modeled as a linear function of carrier density $\alpha_{\rm ai} = \alpha_a(N_i) = K_0 + K_1 N_i$ [11], K_0 and K_1 are the carrier-independent and carrier-dependent absorption loss coefficients, respectively, and K_0 represents the intrinsic material loss. K_1 is mainly due to intervalenceband absorption and free carrier absorption. The carrier-dependent loss is important for considering the effects of using an assist beam. The net modal gain is given in[12] as

$$g_{\omega,i} = g(N_i,\lambda_\omega) = \Gamma(g_{m\omega,i} - \alpha_{\rm ai}) - (1-\Gamma)\alpha_c - \alpha_{\rm scat} = \Gamma g_{m\omega,i} - \alpha_{0i} \quad (6)$$

where α_c and $\alpha_{\rm scat}$ are the loss in the cladding and the scattering loss at heterostructure interfaces, respectively.

A typical buried-heterostructure (BH) SOA operating in the 1.55-μm wavelength is considered for our simulation. Table I shows the simulation and device parameters used in our simulation and the nonlinear (FWM) SOA parameters are summarized in Table II.

TABLE II
NONLINEAR (FWM) SOA PARAMETERS

Symbol	Description	Value	Unit
$P_{s,CH}$	CH induced power saturation	0.69	W^{-1}
$P_{s,SHB}$	SHB induced power saturation	25.5	W^{-1}
α_{CM}	Linewidth enhancement factor by CM	3.2	--
α_{CH}	Linewidth enhancement factor by CH	-3.6	--
α_{SHB}	Linewidth enhancement factor by SHB	24.5	--
τ_{CH}	Carrier heating time	650×10^{-15}	s
τ_{SHB}	Spectral hole burning time	50×10^{-15}	s

B. Mixing Geometry and Coupled Wave Equations

We consider the nondegenerate FWM in an SOA with co-directionally injected pump and signal waves of optical powers P_p and P_s and frequencies ω_p and ω_s, respectively. The FWM interaction between the two beams generates a conjugate signal wave at frequency $\omega_c = 2\omega_p - \omega_s$. Assuming that the signal power is much smaller than the pump power, the other FWM signal at $2\omega_s - \omega_p$ can be neglected. Three relaxation-related gain mechanisms, including carrier density modulation, carrier heating, and spectral hole burning, play key roles for FWM-based wavelength converters [13].

In our model, the wave-mixing between the assist beam and the FWM beams is neglected because of large spacing in the frequency domain between the assist beam and the FWM beams. We attribute the major effect of injecting an assist light to the improvement on the gain saturation characteristic of an SOA. Thus, the effect is considered through (1). The assist light also enhances the effective carrier lifetime, as given by (5), and the saturation intensity for the CM effect. Therefore, the assist light is not included in the following formulation for the FWM process. The influence of adding an assist light on the SHB and CH effects is neglected in our analysis. The saturation powers for carrier heating and spectral hole burning processes are relatively large due to their fast relaxation times.

To simplify the analysis, we adopt a phenomenological model to account for the contribution of various nonlinear mechanisms to the FWM process. A detailed quantum-mechanical analysis can be used for calculating the SHB and CH effects but requires complex formulism. The quasi-steady-state evolution of the pump, signal, and conjugate wave amplitudes $A_j, j = p, s, c$ is given by the coupled equations [13]

$$\frac{dA_s}{dz} = \frac{1}{2}[\{\Gamma\cdot g_{\rm ms}\cdot(1-i\alpha_{\rm CM}) - \alpha_0\} - \Gamma\cdot g_{\rm ms} \cdot(\eta_{\rm sp}|A_p|^2 + \eta_{\rm sc}|A_c|^2)]A_s - \Gamma\frac{g_{\rm ms}}{2}\left[\eta_{\rm pc}A_p^2A_c^*e^{-i\Delta kz}\right] \quad (7)$$

$$\frac{dA_p}{dz} = \frac{1}{2}[\{\Gamma\cdot g_{\rm mp}\cdot(1-i\alpha_{\rm CM}) - \alpha_0\} - \Gamma\cdot g_{\rm mp} \cdot(\eta_{\rm ps}|A_s|^2 + \eta_{\rm pc}|A_c|^2)]A_p - \Gamma\frac{g_{\rm mp}}{2}[(\eta_{\rm sp}+\eta_{\rm cp})A_sA_cA_p^*e^{i\Delta kz}] \quad (8)$$

$$\frac{dA_c}{dz} = \frac{1}{2}[\{\Gamma \cdot g_{\rm mc} \cdot (1 - i\alpha_{\rm CM}) - \alpha_0\} - \Gamma \cdot g_{\rm mc} \cdot (\eta_{\rm cs}|A_c|^2 + \eta_{\rm cp}|A_p|^2)]A_c - \Gamma\frac{g_{\rm mc}}{2}\left[\eta_{\rm ps}A_p^2A_s^*e^{-i\Delta kz}\right] \quad (9)$$

where $\alpha_{\rm CM}$ is the linewidth enhancement factor of an SOA induced by carrier density modulation. We assume that the phase-match condition, $\Delta k = 2k_2 - k_1 - k_3 \approx 0$, is satisfied due to short device length and low dispersion of the SOA [13]. For clarity, the subscript i for section number has been omitted in (7)–(9).

Higher order wave mixing processes between the newly generated waves and the input waves are neglected by assuming that the input pump power is much stronger than the input signal power. Gain saturation due to self-phase modulation-type terms as well as cross-phase modulation-type terms and gain asymmetry are all accounted for in (7)–(9) [13]. The FWM coupling is described in the last terms of (7)–(9), assuming that contributions from CM, SHB, and CH are independent. The coefficients $\eta_{\rm jk}, j, k = p, s, c$ are given by [13]

$$\eta_{\rm jk}(z) = \frac{\left(\frac{1-i\alpha_{\rm CM}}{P_{\rm sat}}\right)}{1 + \frac{P(z)}{P_{\rm sat}} - i(\omega_j - \omega_k)\tau_e} + \sum_{m={\rm CH,SHB}} \frac{\left(\frac{1-i\alpha_m}{P_{s,m}}\right)}{1 - i(\omega_j - \omega_k)\tau_m} \quad (10)$$

where $P(z) = \sum_{\omega=p,s,c,a}|A_\omega(z)|^2$ is the total optical power inside the amplifier. The saturation power for CM is defined by $P_{\rm sat} = E_pA_{\rm cross}/\Gamma a_1\tau_e$, in which the frequency dependence of the gain has been neglected under the assumption that the three beams reside in the vicinity of the gain peak.

From (10), phase interferences between multiple mechanisms cause an asymmetry in the mixing with respect to up- and down-conversion. The relaxation lifetimes are given by τ_e for carrier modulation as well as $\tau_{\rm CH}$ and $\tau_{\rm SHB}$ for heating and hole burning, respectively. The saturation power and linewidth enhancement factor are given for each processes. The term $P(z)/P_{\rm sat}$ appears only in the denominator of the carrier modulation contribution due to the extremely high saturation powers for CH and SHB.

We have taken into account the effect of the assist light by incorporating τ_e in $P_{\rm sat}$. Using an assist light increases $P_{\rm sat}$. The prounced contribution from the assist light is to the gain coefficient $g_{m\omega}$ ($\omega = s, p$, and c). In the previous literature, the gain coefficient is accompanied by $(1 + P/P_{\rm sat})$ in the denominator to account for the gain saturation. Here, as described before, the gain saturation is accounted for by using (1). Under a saturation condition, the optical power depletes carrier density and then decreases the gain. The assist beam can be absorbed and then supplies carriers as the injected light causes severe gain saturation. For example, if the SOA is biased at the current corresponding to the transparent current of the assist beam, the beam generates carriers once the carrier is depleted by the pump or signal beams. The holding of gain by an assist light under large pump and signal powers results in a significant improvement on the FWM efficiency.

C. ASE Noise

One of the main processes to be considered in analyzing an SOA-based wavelength converter is the ASE noise, because it determines the SNR and noise figure of the converter [14]–[18]. The output amplified spontaneous noise power $P_{\rm ASE}$ in a bandwidth of $\Delta\nu$ around optical frequency ν is given by [14]

$$P_{\rm ASE} = h\nu \cdot \Delta\nu \cdot \int_0^L \Gamma g_m(N(z),\nu)n_{\rm sp} \cdot \exp\left\{\int_z^L [\Gamma g_m(N(z),\nu) - \alpha_0] \cdot dz'\right\} \cdot dz \quad (11)$$

where $N(z)$ is the spatial distribution of carrier density and is represented as a constant N_i in each section in our model. $n_{\rm sp}$ is the spontaneous emission factor given by [15]

$$n_{\rm sp} = \frac{N(z)}{N(z) - N_0}. \quad (12)$$

Since the carrier density N_i in the ith section is assumed to be constant, the net gain $G_i(\nu)$ over the section is $G_i(\nu) = e^{g(N_i,\nu)\cdot\Delta L}$. The gain coefficents g_m and g are given in (3) and (6), respectively, but the function form is modified by replacing the argument λ with ν. The ASE power $P_{{\rm ASE},i}$ at optical frequency ν within the bandwidth $\Delta\nu$ at the output of the ith section is obtained by integration of (11) over the section length ΔL for the special case of homogeneous carrier density [16]

$$P_{{\rm ASE},i}(\nu) = G_i(\nu)P_{{\rm ASE},i-1} + h\nu \cdot \Delta\nu \cdot n_{\rm sp} \cdot [G_i(\nu) - 1]\left(\frac{\Gamma g_m(N_i,\nu)}{\Gamma g_m(N_i,\nu) - \alpha_{0i}}\right). \quad (13)$$

The ASE output at the ith section can be divided into two contributions: The first term in (13) represents the amplified ASE noise from the previous section, while the second term is the ASE noise generated within the ith section. The backward propagating ASE power can be calculated similarly by summing up the contributions from the $(i+1)$th section and the current (ith) section.

The ASE recombination rate $R_{{\rm ASE},i}$ in (1) is then given by

$$R_{{\rm ASE},i} = R_{\rm ASE}(N_i) = \sum_\nu \Gamma \cdot g_m(N_i,\nu) \cdot \frac{P_{{\rm ASE},i}(\nu)}{(h\nu) \cdot A_{\rm cross}}. \quad (14)$$

For the numerical calculation, (14) is completed by a finite sum over the 32 spectral slices into which the ASE spectrum is divided. The ASE recombination rate includes the contributions from both the forward and backward propagating ASEs.

D. Numerical Analysis Procedures

As a starting point for the simulation, the carrier densities N_i in each section is obtained using the carrier density rate equation (1) by neglecting the stimulated and spontaneous emission. Solving N_i allows us to calculate the FWM coupling coefficient $\eta_{jk,i}$ as well as the gain coefficient $g_{m\omega,i}$ for every section. The traveling-wave amplitudes $A_{\omega,i+1}$ for the $(i+1)$th section can be calculated by solving the coupled equations (7)–(9), which comprise the FWM interactions. The evolution of the assist light is calculated simply by propagating it from the output end to

the input end. The backward and forward ASEs are calculated using (13) by dividing the major spectral content into 32 uniform slices. The average photon densities $S_{\omega,i}$ are then calculated from $A_{\omega,i}$ and $A_{\omega,i+1}$ using (2), and the ASE recombination rate is calculated using (14). Finally, the carrier densities N_i are updated by iteration using (1). The covergent criterion for the iteration is fulfilled as the right-hand side of (1) reaches less than 10^{-6} for all the sections. In this manner, the fields and injected carrier densities for all sections of the amplifier can be calculated. The profile of the longitudinal field distribution of the amplified signal, injected carrier density, and material gain can also be calculated simultaneously.

III. Transparent Condition and Carrier Distribution

The transparent condition of an SOA corresponds to the condition that the material gain of the SOA is zero for the incident wavelength. The transparent current for an assist light is usually determined from comparing the gain-versus-current curves at a given wavelength between the presence and absence of the assist light. The transparency locates at the intersection of the two curves, since the gain is not changed for the presence of the assist light.

Obviously, the longitudinal profile of the carriers along the active waveguide plays an important role in determining the transparent current of a LHSOA. In this section, we will elucidate the effect of ASE on material gain and the wavelength dependence of transparent current.

A. The Effects of ASE on Transparent Current

To understand the effects of ASE on the transparent current, we compare the gain curves and carrier distribution in two cases, i.e., with and without taking into account the ASE. Fig. 2(a) shows the gain curves at 1550 nm for the cases with and without a 1480-nm assist light, in which the ASE is ignored. The two curves intersect at 102 mA of the bias current, which corresponds to the transparent current for the 1480-nm light. This value is nearly the same as the default material transparent current. The computed carrier density distribution as a function of bias current without ASE is shown in Fig. 2(b). From this figure, it can be seen that the carrier concentration increases with the bias current regardless of whether an assist light is added or not. For the case without an assist light, the carrier density distributes uniformly along the cavity length except for high-bias conditions. The distribution changes if an assist light is injected into the SOA. Below the transparency ($\mathrm{I_{SOA}} < 102$ mA), the assist light of which the wavelength locates at the absorption region will provide carriers near the output facet. In contrast, above the transparency ($\mathrm{I_{SOA}} > 102$ mA), the wavelength of the assist light is located at the gain region, which depletes the carrier near the output facet. Therefore, as we expect, the injection of an assist light can alter the carrier concentration. The deeper the assist light penetrates into an SOA, the less the carrier concentration is altered due to the attenuation of the assist light.

The transparent current refers to the current at which the overall signal gain coefficient is zero. As the ASE is included, Fig. 3(a) shows that the transparent current increases to 105 mA for 1480-nm assist light, which is larger than the default

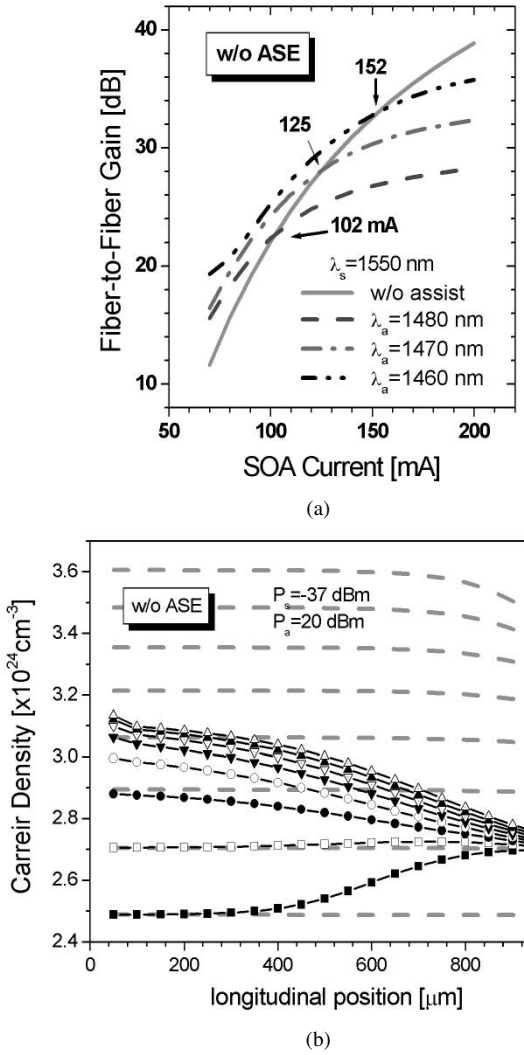

Fig. 2. (a) Gain versus injection current for an SOA under the conditions with and without an assist light. The solid line refers to data without assist light. (b) The computed carrier density distribution inside the active layer of the LHSOA as a function of the applied current with and without an assist light at 1480 nm. The ASE is ignored in this case. Broken curves: without assist light; curves with markers: with assist light. The current varies from 80 to 220 mA with a step of 20 mA.

value. The amplifier gain reduces and the gain saturation comes to occur at a smaller current. We attribute this behavior to the ASE effect and will explain it as follows.

Fig. 3(b) shows the computed carrier density distribution for different bias with ASE being considered. Many features can be observed from this figure. First, well below saturation, the carrier density is uniformly distributed along the longitudinal direction and increases with the applied current. Second, above saturation, the carrier density has a maximum in the middle of the device and minimum at the facets. The carrier profile is symmetrical and is determined by the ASE recombination rate that depletes the carriers near the input and output ends. As the ASE power is strongest at the facets as a result of the amplification action, the recombination rate is also strongest at the facets, leading to a lower carrier density. We can thus conclude that the increased transparent current is mainly a result of the ASE. The ASE consumes carriers near the facets, so more current must be applied to provide the same gain, and this in turn generates

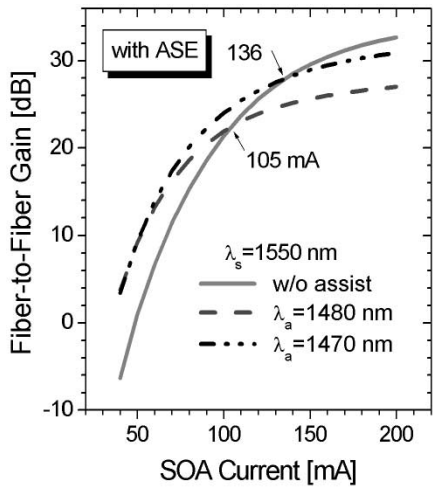

(a)

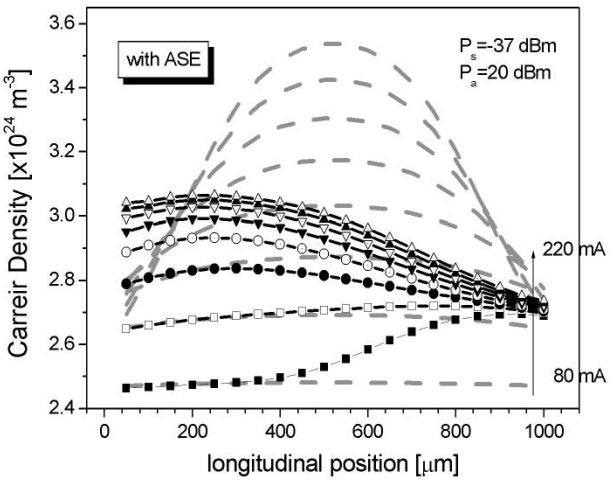

(b)

Fig. 3. (a) Gain versus injection current for an SOA under the conditions with and without an assist light. The solid line refers to data without assist light. (b) The computed carrier density distribution inside the active layer of the LHSOA as a function of the applied current with and without an assist light at 1480 nm. The ASE is included in this case. Broken curves: without assist light; curves with markers: with assist light. The current varies from 80 to 220 mA with a step of 20 mA.

more ASE. As a third point, it can be seen that the nonuniformity of the carrier density distribution increases with the applied current. This is again due to the increase in ASE power with current, which leads to a strong carrier recombination near the facets. As the mean value of the carrier density increases with current, it means that the carrier density decreases toward the facets while it increases in the middle of the active layer, and therefore the nonuniformity of the carrier density distribution increases.

B. Wavelength Dependence of Transparent Point

For wavelength conversion, both the SOA gain and saturation power need to be as high as possible. When a shorter wavelength assist light is used, the SOA can be operated at a higher bias level and still provide transparency to the assist light. Therefore, it is possible to obtain both high conversion efficiency and large improvement from using a short-wavelength assist light. In our scheme, higher injection current is required to make the gain

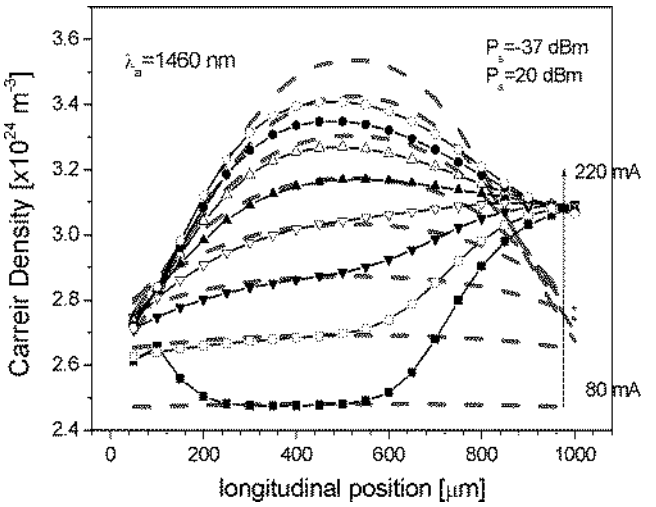

Fig. 4. Computed carrier density distribution along the LHSOA as a function of the applied current with and without an assist light at 1460 nm. Broken curves: without assist light; curves with markers: with assist light. The current varies from 80 to 220 mA with a step of 20 mA.

material transparent for the assist light of shorter wavelength. By doing so, the material gain will increase for the signal and pump beams. A larger output saturation power and the accompanying performance improvement are thus attained due to the increase in the saturation power.

It is worth noting that there is no intersection between the curves with and without a 1460-nm assist light in Fig. 3(a). This was also observed in the experiments. Once again, the effect of ASE makes the cause. Fig. 4 shows that the computed carrier density distribution as a function of the applied current with and without an assist light at 1460 nm. The transparent current is larger for a shorter wavelength of assist light. The ASE enhances with current and in turn enlarges the nonuniformity of the carrier density distribution, leading to the bouncing of the assist light among gain region, transparent point, and absorption region at different sections along the whole cavity. In particular, a shorter wavelength assist light will be located at the absorption region and provide more carriers to increase the amplifier gain as a result of the serious carrier depletion resulted from the strong ASE near the output facet. These effects will accumulate so that the gain could be raised to prevent it from crossing over the gain curve without an assist light.

IV. Static Characteristics of an LHSOA

In this section, we explore the effects of introducing an assist light in SOAs as well as analyze the dependence of the conversion efficiency and SBR on input pump power, input signal power, and wavelength detuning in an LHSOA.

A. Output Saturation Power

As mentioned above, the gain saturation limits the efficiency of SOA-based wavelength converters. The use of an assist light at transparency will maintain the separation of the quasi-Fermi levels and enhances the gain recovery time. The assist light can be transparent in the steady state ($g_{\rm ma} = 0$) and has negative gain after a signal pulse is amplified ($g_a < 0$). As long as the assist light term of (1) is negative, i.e., $g_{\rm ma}P_a < 0$, the recovery

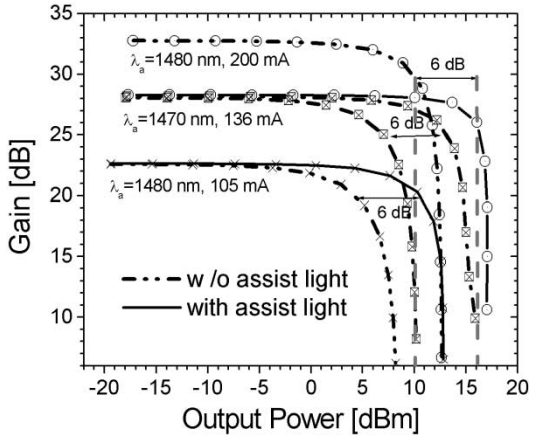

Fig. 5. Comparison of gain versus output power of an SOA for a 1550-nm signal between the absence and presence of an assist light. The solid and dashed curves represent the gain with and without an assist light, respectively. The assist light power is 20 dBm.

time becomes shorter than $\tau_{\rm ei}$. A larger assist power P_a gives a shorter recovery time and hence a larger saturation power.

The gain saturation characteristic of the SOA at different biases with and without a 1480-nm assist light is compared in Fig. 5, where the chip gain is plotted as a function of the signal output power at the facet. The assist light injection improves the saturation output power by 6 dB without reducing the unsaturated gain as the SOA is biases at the transparency for the assist light. The improvement of the gain saturation is also observed at a bias current of 200 mA. In this case, the improvement in gain saturation is accompanied by a reduction in the unsaturated gain. Fig. 5 also shows the improvement on saturation output power from using a 1470-nm assist light at the corresponding transparency. The pump and signal lights experience a larger gain due to an increase in the saturation power by the assist light. This will help to increase the conversion efficiency. We must emphasize that the saturation power at 136 mA with a 1470-nm assist light is larger than that at 200 mA without an assist light. In practical use, applying a smaller bias current can avoid the device degradation induced by the thermal effect that often occurs at higher bias current.

B. Conversion Efficiency

The gain of an SOA can be simply raised by increasing the SOA bias current, but the ultimate gain is limited as a result of the thermal effect and ASE at the high-injection level. On the other hand, adding an assist light can further increase the gain and/or the saturation output power. Fig. 6 shows the conversion efficiency as a function of the wavelength shift for a pump power of -3 dBm and a signal power of -10 dBm. The conversion efficiency is defined as the ratio of the output conjugate signal power to the input signal power. The conversion efficiency decreases at a large detuning frequency because of the frequency response of the nonlinear processes. In addition, the down-conversion efficiency is higher than the up-conversion efficiency. This is due to the wavelength dependent gain and partially destructive/constructive phase interference among the FWM mechanisms.

Fig. 7 shows the calculated conversion efficiency as a function of the input pump power for different signal power without

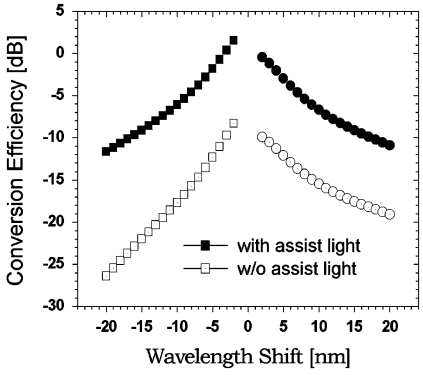

Fig. 6. Conversion efficiency as a function of wavelength shift (signal power $=-10$ dBm, pump power $=-3$ dBm) with and without an assist light.

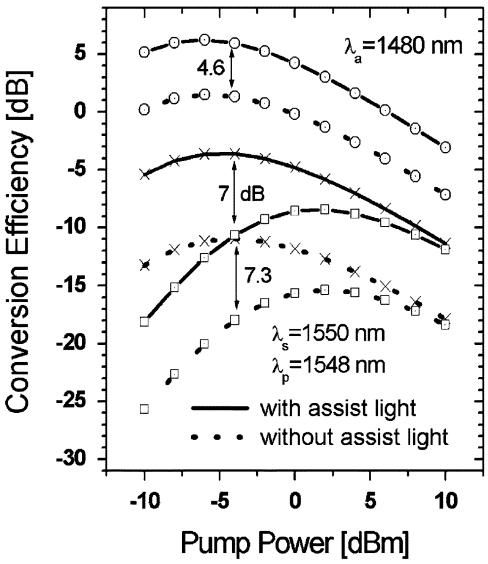

Fig. 7. FWM conversion efficiency of an SOA under the conditions with and without an assist light. The solid and dashed lines represent "with" and "without" the injection of an assist light, respectively. Circles: bias current $I = 200$ mA, $P_s = -10$ dBm; crosses: $I = 105$ mA, $P_s = -10$ dBm; squares: $I = 105$ mA, $P_s = -3$ dBm.

and with an assist light of 20-dBm power at a wavelength shift of 4 nm. Increasing the pump power can raise the conversion efficiency, but the conversion efficiency decreases with the pump power after the SOA encounters severe gain saturation.

In these figures, the conversion efficiency is up-shifted with the injection of an assist light. That is, the maximal conversion occurs for almost the same pump power but the efficiency increases as the assist light is present. The effective carrier lifetime is reduced by introducing an assist light and in turn extends the output saturation power of the SOA. Improved FWM conversion efficiency is thus benefited from these advantageous effects.

C. SBR

The SBR is crucial for evaluating the feasibility of an SOA-based wavelength converter. The SBR is defined as

$$\mathrm{SBR} \cong \frac{P_c(L)}{P_{\rm ASE}(L)} = \frac{\eta_{\rm CE} P_s(0)}{P_{\rm ASE}(L)} \tag{15}$$

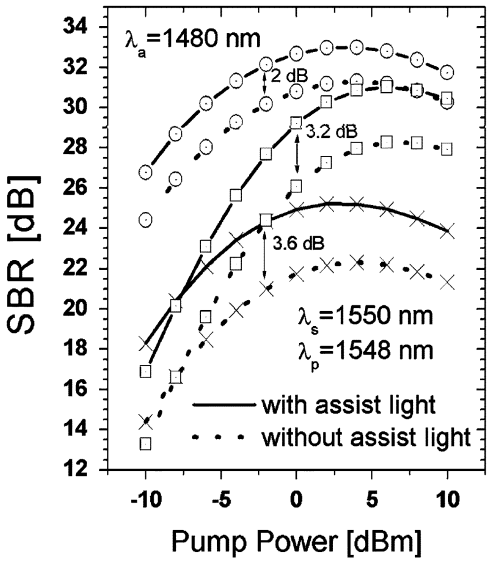

Fig. 8. SBR of an SOA wavelength converter under the conditions with and without an assist light. The solid and dashed lines represent "with" and "without" the injection of an assist light, respectively. Circles: $I = 200$ mA, $P_s = -10$ dBm; crosses: $I = 105$ mA, $P_s = -10$ dBm; squares: $I = 105$ mA, $P_s = -3$ dBm.

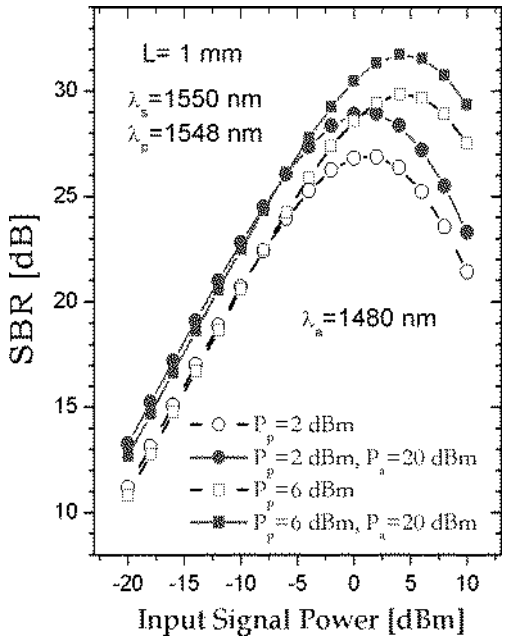

Fig. 9. SBR of an SOA for wavelength down-conversion of 4 nm under the conditions with and without an assist light. The solid and dashed lines represent "with" and "without" the injection of an assist light, respectively.

where $P_{\mathrm{ASE}}(L)$ is the ASE power measured at the converted wavelength λ_c within a certain optical bandwidth at the SOA output.

Fig. 8 shows the dependence of SBR on the pump power. The result shows a maximum beyond which the SBR decreases with saturation. If we describe the conversion efficiency as $\eta_{\mathrm{CE}} = G_p^2 \cdot G_s \cdot P_p^2 \cdot R(\Delta\lambda)$ [19], then the expression of the SBR is given by

$$\mathrm{SBR} \cong \frac{G_p^2 \cdot G_s \cdot P_p^2 \cdot P_s \cdot R(\Delta\lambda)}{(G_c - 1) \cdot h\upsilon \cdot n_{\mathrm{sp}} \cdot B_0} \tag{16}$$

where $R(\Delta\lambda)$ depends only on the detuning between the pump and signal wavelengths and B_0 is the optical bandwidth of the filter. $G_\omega(\omega = p, s, c)$ stands for the chip gain of the pump, signal, and conjugate beams. To roughly estimate the trend of the SBR against pump power and gain, the chip gains are all approximated to be G. Thus, (16) indicates that the SBR varies approximately in the form of $G^2 \cdot P_p^2 / n_{\mathrm{sp}}$ for a given P_s. Below the saturation, G and n_{sp} are constant, so the SBR is proportional to P_p^2. In deep saturation, G is inversely proportional to P_p, giving an almost constant $G^2 \cdot P_p^2$ product. Consequently, the SBR decreases due to the increase in n_{sp}. Therefore, the SBR reaches a maximum at a moderate pump level. The optimal pump power for maximal conversion efficiency is different from the optimal one for maximal SBR. This trend is consistent with the literature. The SBR is again improved by applying an assist light. This improvement is regarded as an extra benefit provided by the assist light, in addition to its enhancement on the conversion efficiency. The scale and trend of performance improvement are very consistent with the experimental results [7].

Fig. 9 shows the calculated output SBR as a function of the input signal power. The pump powers are 2 and 6 dBm, corresponding approximately to the values that provide maximal CE and SBR, respectively. The results indicate that with 6-dBm pump power and an assist light the output SBR can reach a maximum of 33 dB. The optimal input signal power for the best SBR shifts from 2 to 5 dBm as an assist light is applied. This again reveals the benefits of using an assist light. Since the saturation power is increased, larger pump and signal powers are allowed to propagate in the SOA. This can improve the conversion performance. A typical problem of using an SOA with a high input power is the pattern-dependent distortion and intersymbol interference (ISI) due to the finite gain recovery time of the amplifier [20]. Injecting an assist light at transparency can promote the gain recovery without reducing the amplifier gain, which will be useful for reducing the ISI when the input signal power is higher.

V. Choice of Device Length

As a starting point, $\eta_{\mathrm{CE,max}} \propto G_0 \cdot P_{\mathrm{sat}}^2$ is usually considered for optimizing the amplifier geometry. Of particular interest is the question if an increase in L, and consequently in G_0, could be a good way to increase the maximum efficiency. The answer is not so evident as it could see and requires further investigation. Indeed, the increase in L brings about a stronger reduction of the carrier density along the propagation direction. P_{sat} depends on the carrier density, therefore it changes along the propagation direction. The longer the amplifier is, the stronger this effect. Thus, the assumption of a constant P_{sat} is no longer correct in long devices. Here, we compare the device performance for different lengths of SOAs by keeping the carrier density constant. That is, a current proportional to the device length is applied, and then G_0 as well as the input saturation power are determined to calculate the maximum conversion efficiency and SBR as a function of pump power for various device lengths.

Fig. 10 reports the efficiency as a function of the pump power for different values of L. The beneficial effects of greater L on conversion efficiency are apparent. For each device, the values have been obtained for a current proportional to the length (120

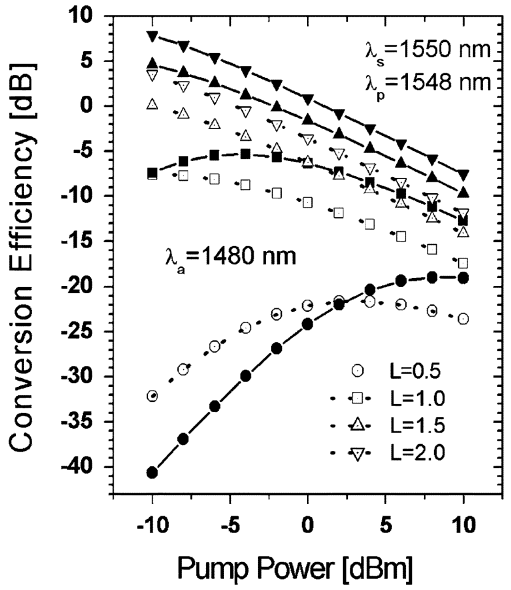

Fig. 10. FWM efficiency versus the pump power for a LHSOA. Data are for 4-nm wavelength down-conversion. Solid and empty symbols represent the results with and without an assist light, respectively. Circles: $\mathrm{L} = 0.5$ mm; squares: $\mathrm{L} = 1$ mm; up triangles: $\mathrm{L} = 1.5$ mm; down triangle: $\mathrm{L} = 2$ mm.

TABLE III
SIMULATION PARAMETERS FOR DEVICE OPTIMIZATION

L_{SOA} (mm)	0.5	1	0.5	1	1.5	2
I_{SOA} (mA)	51	110	60	120	180	240
G_0 (dB)	13	27	15	28	34	34
			(13)	(27)	(36)	(39)
$P_{in,sat}$ (dBm)	-5	-18	-6	-18	-23	-23
	(2.5)	(-12)	(3)	(-10)	(-20)	(-21)

The number in the parenthese is derived under the condition with an assist light at 1480 nm being injected.

mA/mm). Table III summarizes the unsaturated gain and input saturation power for SOAs without and with an assist light (data in parenthesis). We note that the gain gradually reaches a maximum as the SOA converter is getting longer. This results from the saturation induced by the strong ASE. However, the device performance can still be improved because of the presence of a very strong pump. This feature explains why the efficiency increases with increasing L. In absence of a strong saturation by the ASE, as in the short amplifiers, the efficiency arrives at a maximum when gain saturates. In contrast, the curves for longer devices show a maximum at smaller pump powers. This is due to a larger gain and the presence of very strong ASE.

Fig. 11 reports the SBR as a function of the pump power for different values of L. Significant improvement of the SBR can be obtained by injecting an assist light. For a shorter device, because of the low gain, the pump power at the output may not be high enough to saturate the amplifier. The converter output is proportional to the square of the pump power and the signal power. This is in agreement with the square dependence of SBR on pump power, as shown in Fig. 11 for the 0.5-mm amplifier. The SBR at high pump power is worse for a longer SOA because of stronger gain saturation and larger ASE.

Injecting an assist light can improve both conversion efficiency and SBR for all the cases shown in Figs. 10 and 11. For example, the conversion efficiency and SBR can be -7 and

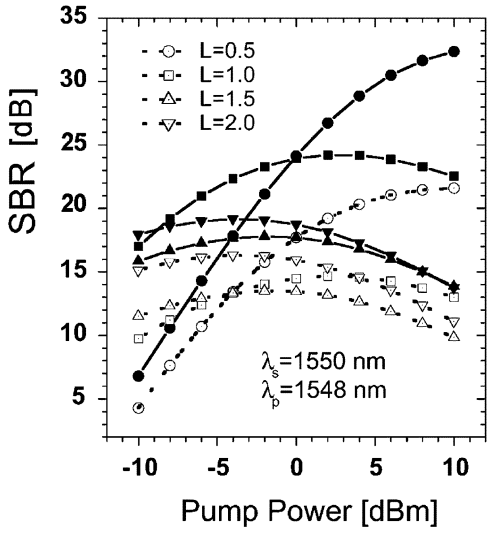

Fig. 11. SBR versus the pump power for a LHSOA. Data are for 4-nm wavelength down-conversion. Solid and empty symbols represent the results with and without an assist light, respectively. Circles: $\mathrm{L} = 0.5$ mm; squares: $\mathrm{L} = 1$ mm; up triangles: $\mathrm{L} = 1.5$ mm; down triangle: $\mathrm{L} = 2$ mm.

24 dB, respectively, for a 1-mm-long SOA with 2-dBm pump power. The assist light has a more remarkable effect on shorter SOAs. Nevertheless, long SOAs yield higher conversion efficiency. This indicates that a compromise between the conversion efficiency and SBR must be made to assure the system performance. In practical use, low noise degradation of the signal characteristics is strictly required for a wavelength converter because a signal may be converted more than once within the network. Thus, it is more important to optimize the SBR than η_{CE} for applications requiring multiple stages of wavelength conversion. Consequently, a short SOA is preferred and using an assist light can make big difference by improving the SBR. On the other hand, long SOAs can be used for single-stage wavelength conversion. Even in this case, an assist light can still enhance both the conversion efficiency and SBR.

VI. CONCLUSION

We have investigated theoretically the performance of a wavelength converter using an SOA and a CW assist light. Our simulation method took into account the FWM mechanisms, ASE noise, longitudinally variation of the carrier density due to SHB, and wavelength-dependent gain. The nonuniformity of carrier density distribution resulted from the ASE explains the shift in the transparent current for a large bias current. It is shown that the conversion efficiency can be improved by more than 6 dB when the SOA is biased at the transparent current for 20 dBm of 1480-nm assist light. The assist light can also improve the SBR by about 3 dB. These theoretical results are very consistent with the published experimental results. The analysis can be applied to optimize the effects of using an assist light in order to improve the performance of SOA-based wavelength converters. It can also be extended to analyze the dynamic response of a LHSOA.

Using an assist beam can provide greater improvement of the wavelength conversion performance as the SOA is biased at the corresponding transparency for the assist beam. Under

our scheme, through the injection of a shorter wavelength assist light, one can expect performance improvements at higher bias current and gain, which is needed for high-efficiency and low-noise FWM wavelength conversion. The analysis suggests that an assist light can provide significant improvement on the SBR for a short SOA. To assure the system performance, a compromise between the conversion efficiency and SBR must be made for choosing the optimal device length.

REFERENCES

[1] D. F. Geraghty, R. B. Lee, M. Verdiell, M. Ziari, A. Mathur, and K. J. Vahala, "Wavelength conversion for WDM communication systems using four-wave mixing in semiconductor optical amplifiers," *IEEE J. Select. Topics Quantum Electron.*, vol. 3, pp. 1146–1155, Oct. 1997.

[2] S. J. B. Yoo, "Wavelength conversion technologies for WDM network applications," *J. Lightwave Technol.*, vol. 14, pp. 955–966, 1996.

[3] A. D'Ottavi, F. Girardin, L. Graziani, F. Martelli, P. Spano, A. Mecozzi, S. Scotti, R. Dall'Ara, J. Eckner, and G. Guekos, "Four-wave mixing in semiconductor optical amplifiers: A practical tool for wavelength conversion"," *IEEE J. Select. Topics Quantum Electron.*, vol. 3, pp. 522–528, 1997.

[4] M. A. Dupertuis, J. L. Pleumeekers, T. P. Hessler, P. E. Selbmann, B. Deveaud, B. Dagens, and J. Y. Emery, "Extremely fast high-gain and low-current SOA by optical speed-upat transparency," *IEEE Photon. Technol. Lett.*, vol. 12, pp. 1453–1455, 2000.

[5] J. Yu and P. Jeppesen, "Improvement of cascaded semiconductor optical amplifier gates by using holding light injection," *J. Lightwave Technol.*, vol. 19, pp. 614–623, 2001.

[6] M. Usami, M. Tsurusawa, and Y. Matsushima, "Mechanism for reducing recovery time of optical nonlinearity in semiconductor laser amplifier," *Appl. Phys. Lett.*, vol. 72, pp. 2657–2659, 1998.

[7] S. L. Lee, P. M. Gong, and C. T. Yang, "Performance enhancement on SOA-based four-wave-mixing wavelength conversion using an assisted beam," *IEEE Photon. Technol. Lett.*, vol. 14, pp. 1713–1715, 2002.

[8] S. Scotti, L. Graziani, A. D'Ottavi, F. Martelli, A. Mecozzi, P. Spano, R. Dall'Ara, F. Girardin, and G. Guekos, "Effects of ultrafast processes on frequency converters based on four-wave mixing in semiconductor optical amplifiers," *IEEE J. Select. Topics Quantum Electron.*, vol. 3, pp. 1156–1161, Oct. 1997.

[9] A. E. Willner and W. Shieh, "Optimal spectral and power parameters for all optical wavelength shifting: Single stage, fanout, and cascadability," *J. Lightwave Technol.*, vol. 13, pp. 771–781, May 1995.

[10] N. Storkfelt, B. Mikkelsen, D. S. Olesen, M. Yamaguchi, and K. E. Stubkjaer, "Measurement of carrier lifetime and linewidth enhancement factor for 1.5-μm ridge-waeguide laser amplifier," *IEEE Photon. Technol. Lett.*, vol. 3, pp. 632–634, 1991.

[11] *Handbook of Semiconductor Laser and Photonic Integrated Circuits*, Chapman & Hall, London, U.K., 1994.

[12] G. P. Agrawal and N. K. Dutta, *Semiconductor Lasers*, New York: Van Nostrand, 1993.

[13] N. C. Kothari and D. J. Blumenthal, "Influence of gain saturation, gain asymmetry, and pump/probe depletion on wavelength conversion efficiency of FWM in semiconductor optical amplifiers," *IEEE J. Quantum Electron.*, vol. 32, pp. 1810–1816, Oct. 1996.

[14] K. Obermann, I. Koltchanov, K. Petermann, S. Diez, R. Ludwig, and H. G. Weber, "Noise analysis of frequency converters utilizing semiconductor optical amplifiers," *IEEE J. Quantum Electron.*, vol. 33, pp. 81–88, Jan. 1997.

[15] T. Mukai, Y. Yamamto, and T. Kimura, "S/N and error rate performance in AlGaAs semiconductor laser preamplifier and linear repeater systems," *IEEE Trans. Microwave Theory Tech.*, vol. MTT-30, pp. 1548–1556, Oct. 1982.

[16] M. A. Summerfield and R. S. Tucker, "Frequency-domain model of multiwave mixing in bulk semiconductor optical amplifiers," *IEEE J. Select. Topics Quantum Electron.*, vol. 5, pp. 839–850, May–June 1999.

[17] C. H. Henry, "Theory of spontaneous emission noise in open resonators and its application to lasers and optical amplifiers," *J. Lightwave Technol.*, vol. LT-4, pp. 288–297, Mar. 1986.

[18] A. J. Lowery, "Amplified spontaneous emission in semiconductor laser amplifiers: Validity of the transmission line laser model," *Proc. Inst. Elect. Eng.*, pt. J, vol. 137, pp. 241–247, Aug. 1990.

[19] J. Zhou, N. Park, J. W. Dawson, K. J. Vahala, M. A. Newkirk, and B. I. Miller, "Efficiency of broadband four-wave mixing wavelength conversion using semiconductor traveling-wave amplifiers," *IEEE Photon. Technol. Lett.*, vol. 6, pp. 50–52, Jan. 1994.

[20] G. Eisenstein, P. B. Hansen, J. M. Wiesenfeld, R. S. Tuker, and G. Raybon, "Amplification of high repetition rate picosecond pulses using an InGaAsP traveling-wave amplifier," *Appl. Phys. Lett.*, vol. 53, pp. 1539–1541, Oct. 1988.

Pei-Miin Gong was born in Taipei, Taiwan, in 1978. She received the B.S. degree in electronic engineering from Tarn Kang University, Taipei, Taiwan, in 2000 and the M.S. degree in electronic engineering from National Taiwan University of Science and Technology, Taipei, Taiwan, in 2002.

In 2002, she joined Computer & Communications Research Laboratory, Industrial Technology Research Institute, Hsinchu, Taiwan, where she works on wavelength conversion with semiconductor devices.

Jyh-Tsung Hsieh received the B.S. degree from the National Cheng Kung University, Tainan, Taiwan, in 1990 and the M.S.E.E. and Ph.D. degrees in electrical engineering from the Tsing Hua University, Hsinchu, Taiwan, in 1992 and 2000, respectively.

Since October 2000, he has been working as a Post-Doctoral Fellow at the Graduate Institute of Communication Engineering, National Taiwan University, Taipei, Taiwan. In 1999, he was a Visiting Scientist at the University of Stuttgart, Stuttgart, Germany. His research interests have been surface science of semiconductors, III-nitride based semiconductor materials and devices, semiconductor optical amplifiers, and photonic integrated circuits.

San-Liang Lee (S'92–M'95) received the B.S. degree in electronics engineering from National Chiao Tung University, Hsinchu, Taiwan, in 1984, the M.S. degree in electrical engineering from National Taiwan University, Taipei, in 1986, and the Ph.D. degree in electrical and computer engineering from the University of California, Santa Barbara (UCSB), in 1995.

He joined the faculty of the Department of Electronic Engineering, National Taiwan University of Science and Technology (NTUST), Taipei, in 1988. He became an Associate Professor in 1995 and a Professor in 2002. He was on leave from NTUST and worked for the Ph.D. degree at UCSB from 1991 to 1995. He is currently Director of the Center for Optoelectronic Science and Technology, College of Electrical and Computer Engineering, NTUST. His research interests include optoelectronic components, photonic integrated circuits, and optical switching technologies. He has published more than 50 refereed papers in international journals and conferences and holds four patents.

Dr. Lee is a member of the IEEE Laser and Electro-Optic Society and the IEEE Communication Society.

Jingshown Wu (S'73–M'78–SM'99) received the B.S. and M.S. degrees in electrical engineering from National Taiwan University, Taipei, 1970 and 1972, respectively, and the Ph.D. degree from Cornell University, Ithaca, NY, in 1978.

He joined Bell Laboratories in 1978, where he worked on digital network standards and performance and optical fiber communication systems. In 1984, he joined the Department of Electrical Engineering of National Taiwan University as a Professor and was the Chairman of the Department from 1987 to 1989. He was also the Director of the Communication Research Center, College of Engineering, of the university from 1992 to 1995. From 1995 to 1998, he was the Director of the Division of Engineering and Applied Science, National Science Council, R.O.C., on leave from the university. From 1999 to 2002, he was the Chairman of the Commission on Research and Development and the Director of the Center for Sponsor Programs of the university. Currently he is the vice-president of the University. He is interested in optical fiber communications, computer communications, and communication systems. He has published more than 100 journal and conference papers and holds 12 patents.

Prof. Wu is a Life Member of the Chinese Institute of Engineers, the Optical Society of China, and the Institute of Chinese Electrical Engineers. Since 1997 he has served as the Vice Chairman (1997–1998) and the Chairman (1998–2000) of IEEE Taipei Section.